Caving 2026 – A van As, D Cumming-Potvin & J Wesseloo (eds)
© 2026 Australian Centre for Geomechanics, Perth, ISBN 978-1-7636842-3-2
doi:10.36487/ACG_repo/2645_39

Rock mechanics study on block caving design following open pit mining: a case study of Yandong copper mine

Xiong Zanmin [a,b,*], Liu Yuming [a,b], Liang Mingchun [a,b], Li Wen [a,b], Li Xiaolong [a,b], Ren Pengzhao [a,b], Xia Changnian [a,b]

[a] *China ENFI Engineering Corporation, China*

[b] *Key Laboratory of Ground Control Management Plan in Deep Metal Mines National Mine Safety Administration, China*

Abstract

The application of open pit and block caving combined (OPBC) mining is an extremely challenging task, particularly under complex orebody occurrence conditions. For thick, low-grade deposits with shallow to medium orebody depths, OPBC represents the most economical mining method. Taking the Yandong copper mine as the engineering background, this study is a rock mechanics study on the applicability of OPBC and demonstrates a stepwise methodology for the assessment and safe recovery of OPBC method at the Yandong copper deposit, including the determination of open pit slope angle and mining depth, investigation of ore-rock mass structure, caveability evaluation and simulation analysis of progressive failure of the open pit slope during underground mining using Flac3D. The study demonstrates that implementing OPBC at the Yandong copper mine is feasible under the evaluated geological conditions, and the results can serve as a reference for the design of similar mines.

Keywords: *open pit and block caving combined mining, caveability evaluation, progressive failure, caving-induced subsidence, mine design*

1 Introduction

Adopting an open pit combined underground mining approach for mineral resource development can both reduce initial investment and achieve best resource utilisation. When the ore and rock mass exhibit good caveability, block cave mining methods to extract massive, low-grade orebodies are increasingly gaining attention from the mining industry given their merits in terms of safety, tonnages produced and mining costs that can match those of open pit operations. The mining method involves the undercutting and bulk extraction of ore through caving (Brown 2003, 2004), which in turn leads to the slip of the pit above the propagating cave (Flores & Karzulovic 2003). However, the stability of slopes and the caving process during block cave mining pose challenges in mining design (Woo et al. 2009). Accurately assessing slope damage during the reasonable ore release process to meet production requirements and ensure operational safety is of great significance for the design of open pit and block caving combined (OPBC) mining (Moss et al. 2006).

For combined mining methods, the problems related to rock mass stability differ significantly from those encountered in single mining method operations (Bakhtavar et al. 2009). Numerical simulations were employed to investigate slope stability under combined mining operations, including backfill mining (Zhang et al. 2013), room-and-pillar mining (Wang et al. 2022) and sublevel caving (Wang & Zhong 2013; Fu et al. 2026). For block caving, simulating the migration of caved material to fill voids is a critical issue (Sainsbury 2010). Tegachouang et al. (2021) employed artificial backfilling to study the influence of the backfill materials on the stability of an open pit during underground block caving mining. Yuan et al. (2024) simulated the caving process of the surrounding rock around the caved body using the strain softening criterion. Specifically, the rock unit is transformed into the rubble unit once the equivalent plastic strain reaches a critical value. The CaveHoek constitutive model (Pierce 2013) was developed to simulate the progressive failure and

[*] Corresponding author. Email address: xiongzm@enfi.com.cn

disintegration of rock masses as they transition from an intact or jointed state to caved material, while accounting for draw-induced bulking and the associated softening of the deformation modulus. Regarding brittle rock behaviour, a new strain softening model named IMASS (Itasca Model for Advanced Strain Softening) has been created (Ghazvinian et al. 2020).

This project conducted an engineering geological survey, designed the slope angle rationally, and employed the IMASS constitutive model to analyse the rock mass caving process. The caving failure was simulated and research was undertaken to define how damage evolves in caving rock masses. The findings were applied to design and provided guidance for mine production.

2 Engineering background

2.1 Overview of the mining area

The Yandong copper deposit is a porphyry deposit, with the orebodies generally trending nearly east–west. Located 120 km southwest of Hami City, the orebodies primarily develop in monzonitic porphyry and andesite, with the surrounding rocks sharing the same lithology as the orebodies. Due to limited structural influence in the mining area, the rock mass is mainly affected by weathering. The rock mass integrity progressively improves with depth increase.

The terrain within the mining area has minimal undulation, with a maximum elevation of +779 m and a minimum of +550 m. It belongs to the low mountain and hilly geomorphological type. The region experiences a typical continental climate characterised by cold winters, hot summers, frequent winds in spring and autumn, significant temperature variations and water scarcity. There are no perennial surface water bodies or rivers. Only temporary surface run-off occurs due to rainfall convergence, with a very small portion infiltrating underground.

2.2 Structural features of mining area

No regional or large-scale faults are developed in the mining area, indicating a simple geological structure. Three groups of faults striking east–west, northeast–southwest and northwest–southeast are present but occur mostly in the southeastern part. Only a few of these faults directly affect the orebody or surrounding rock. The Kangurtag Fault Zone runs through the southeastern part of the mining area, with an overall strike of nearly east–west and a dip angle of about 70° towards the south. It is a northern boundary fault of the ductile shear zone. No significant damage was found to the orebody due to various structural features within the area.

The folds in the area are sparse, and the overall structure is a northeast to east trending, south dipping monocline. The exposed strata are three lithological segments of the Qishan Group. The deposit is located in the Carboniferous intrusive plagioclase granite porphyry and its contact zone with the first lithological segment of the second group of the Carboniferous Penguin Mountain Group. The attitude of the orebody is similar to that of the plagioclase granite porphyry and surrounding rock and is significantly controlled by the intrusion of the rock mass.

2.3 Orebody characteristics

The orebody mainly occurs in plagioclase granite porphyry and is also distributed in surrounding rocks such as andesite and diorite porphyry. The orebody has a simple morphology, appearing in layered, plate-like and vein-like forms.

The overall orebody is about 3,000 m long, with widths of 300 m in the northeast and 1,400 m in the southwest. It consists of more than 100 ore lenses, distributed in two main ore-bearing layers. Each orebody is controlled by a synclinal structure, with a northeast direction of 48 to 88° and a steep slope towards the northwest wing and a gentle slope towards the southeast wing. The northeast end of the slope tilts upwards, while the southwest end tilts downwards at an angle of 20°. The orebody morphology is shown in Figure 1.

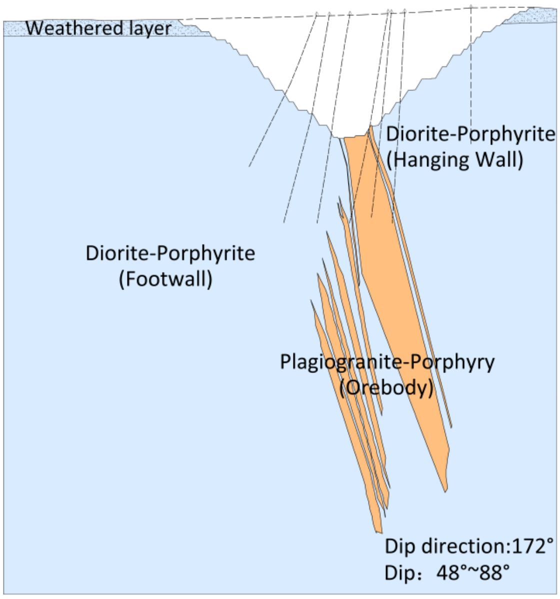

Figure 1 Orebody morphology of Yandong copper mine

3 Caveability evaluation

3.1 Engineering geological survey

Based on core logging of the exploration boreholes, the average rock quality designation (RQD) value within the 0–200 m depth range is 42.3, indicating poor rock mass quality. Within the 200–500 m depth range, the average RQD value is 50.5, indicating fair rock mass quality. Below 500 m depth, the average RQD value is 71.5, indicating further improvement in rock mass integrity. The statistical results of RQD along the depth direction are shown in Figure 2.

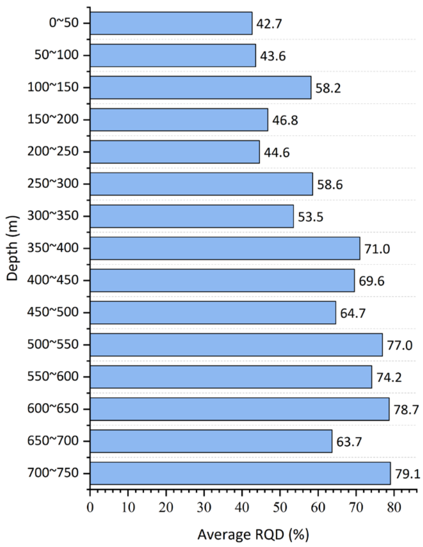

Figure 2 Average RQD along the depth direction

The dip angles of the structural planes revealed by the supplementary drilling are mostly between 45° and 75° (Figure 3a). The dominant structural planes of ZKBC-1 borehole located in the lower part of the orebody, ZKBC-4 borehole located on the east side of the mining area, and ZKBC-5 borehole located inside the orebody tend to have similar orientations, mainly in the near-N and near-S directions, and their orientations are roughly consistent with the orientation of the orebody. The structural planes of ZKBC-2 borehole located on the upper wall of the orebody and ZKBC-4 borehole on the west side of the mining area have no obvious dominant tendency.

Overall, the occurrence of structural planes in the mining area is closely related to the occurrence of the orebody, and the internal structural components of the orebody tend to be roughly consistent with the orebody. Overall, the density of structural planes in the five boreholes is not high, and the integrity of the rock mass is good. The density of structural planes in the five boreholes is generally less than 5 per metre throughout the entire borehole range, with a total of 10–50 structural planes per 10 m. The linear density of rock structural planes buried shallower than 200 m is relatively high, with an average of about 4 discontinuities per metre; the linear density of areas buried deeper than 200 m is relatively low, with an average of about 2–3 discontinuities/m (Figure 3b). The discontinuity surfaces are all wavy, mainly rough and smooth, with rough fracture surfaces accounting for 63% and smooth fracture surfaces accounting for 37%.

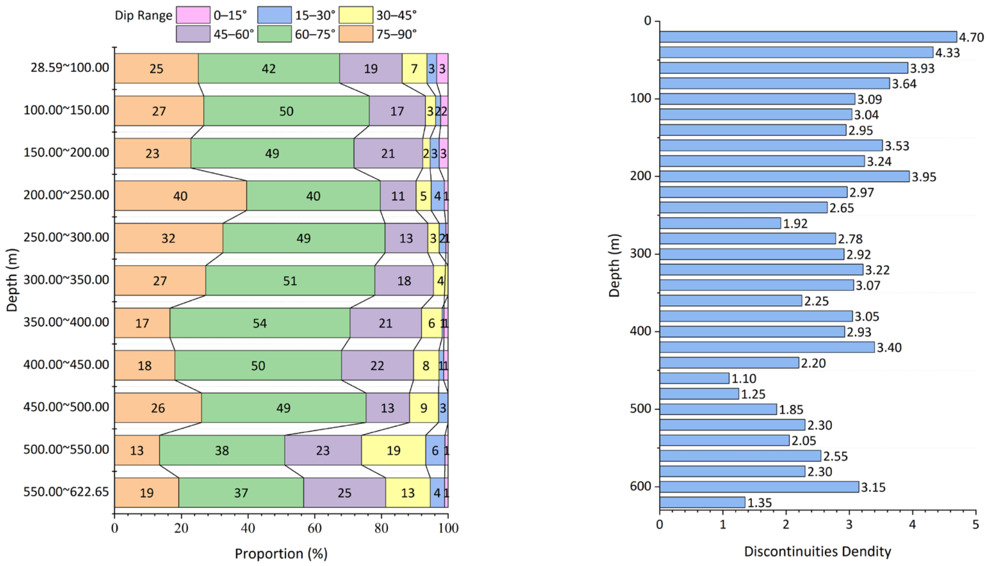

(a) (b)

Figure 3 Dip and density of structural planes. (a) Dip distribution; (b) Discontinuity density

3.2 Analysis of in situ stress characteristics

The hydraulic fracturing method was used to measure the geostress in the Yandong copper mine area. The measured values of geostress in three test holes showed that the maximum principal stress direction in the shallow area below an elevation of 150 m was N35.05°–60.63° E, and the maximum principal stress direction in the deep area below an elevation of 150 m changed to N42.16°–72.47° W. The vertical in situ stress is assumed to be overburden stress, and the horizontal in situ stress is approximately linearly correlated to the depth, as shown in Equations (1) and (2).

$$S_{\mathrm{H}} = 0.0314h + 8.168 \tag{1}$$

$$S_{\mathrm{h}} = 0.0208h + 4.096 \tag{2}$$

where:

S_H = maximum horizontal principal stress (MPa)

S_h = minimum horizontal principal stress (MPa)

h = depth (m).

3.3 Rock mass quality classification

According to the rock mass quality classification standards, a mining rock mass rating (MRMR) rock mass quality evaluation was conducted on the mining area. The MRMR values of the rock mass range from 20 to 60, indicating poor to fair quality. Using Laubscher's caveability chart (Laubscher 1994), the initial caving hydraulic radius for the surrounding rock and orebody is calculated to range from 6 m to 17 m, while the sustained caving hydraulic radius ranges from 15 m to 30 m. Taking borehole ZKBC-5 as an example, the average MRMR varies with depth (Figure 4a). The corresponding caving hydraulic radius shown in Figure 4b is relatively high in both the shallow and deep sections (around 53–56) but drops to a minimum of approximately 29 in the 200–300 m depth range. This lower rock mass quality in the intermediate zone is favourable for block cave mining.

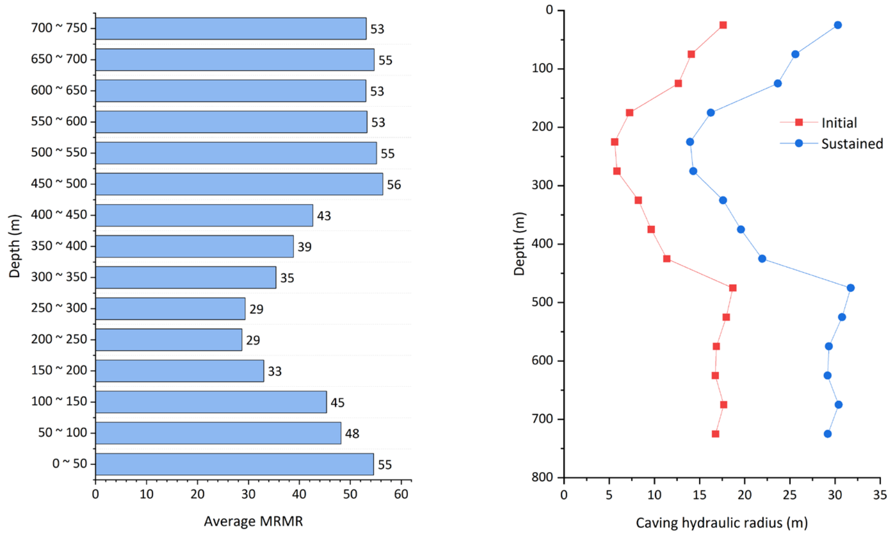

(a) (b)

Figure 4 Average MRMR and caving hydraulic radius of borehole ZKBC-5 along the depth direction. (a) Average MRMR; (b) Caving hydraulic radius

For the block caving area planned for Yandong copper mine, the volume and average MRMR values of different MRMR rock mass qualities of the orebody and surrounding rock were statistically analysed. The statistical results are shown in Table 1.

Table 1 Statistics of MRMR values and caveability of orebody and rock

Rock type	MRMR range	Proportion (%)
Ore	0–20	0
	21–40	80
	41–60	20
	61–80	0
Surrounding rocks	0–20	0
	21–40	64
	41–60	36
	61–80	0

3.4 Caveability evaluation

The caveability assessment of the Yandong copper deposit indicates favourable conditions for block caving mining, as supported by the integrated analysis of orebody geometry, rock mass quality and structural setting.

The orebody displays considerable thickness and steep dip characteristics, which are geometrically conducive to cave initiation, propagation and sustainable drawpoint operations. The RQD statistics demonstrate depth-dependent variability, with average values of 42.3 (0–200 m) and 50.5 (200–500 m), reflecting progressively improving rock mass integrity with depth; nevertheless, the moderate to poor RQD in the upper and middle sections supports the feasibility of block caving. Rock mass quality based on the MRMR system ranges from 20 to 60, classifying the rock mass as poor to fair quality that is inherently amenable to caving.

The dominant structural planes dip at angles between 45° and 75°, with orientations largely consistent with the orebody attitude. This structural configuration promotes controlled fracturing and facilitates gravity-driven caving. Moreover, the mining area exhibits a simple geological structure devoid of regional-scale faults that directly affect the orebody, minimising structural interference and ensuring favourable conditions for large-scale caving extraction. Importantly, the in situ stress regime is dominated by horizontal stress, which promotes stress redistribution and fracturing upon undercutting, thereby enhancing cave initiation and propagation. These geotechnical conditions confirm the suitable caveability for block caving mining.

4 Mining design status

4.1 Open pit mining design

As designed, the open pit mining final pit limit has a maximum mining elevation of +734 m, a minimum mining elevation of 450 m, an ore transport portal elevation of +704 m, and a waste rock transport portal elevation of +706 m. The open pit has a maximum top opening dimension of 1,600 m in length and 690 m in width, with a bottom opening dimension of 350 m in length and 50 m in width. The pit crest elevation of the open pit is +690 m. The final slope height ranges from 254 m to 284 m, with the southern slope being the highest. Based on factors including engineering geology, rock groups, slope height and rock mass quality grades, the open pit slope of Yandong copper mine is divided into four slope engineering zones. The open pit mining final pit boundary and the slope angle zoning situation are shown in Figure 5.

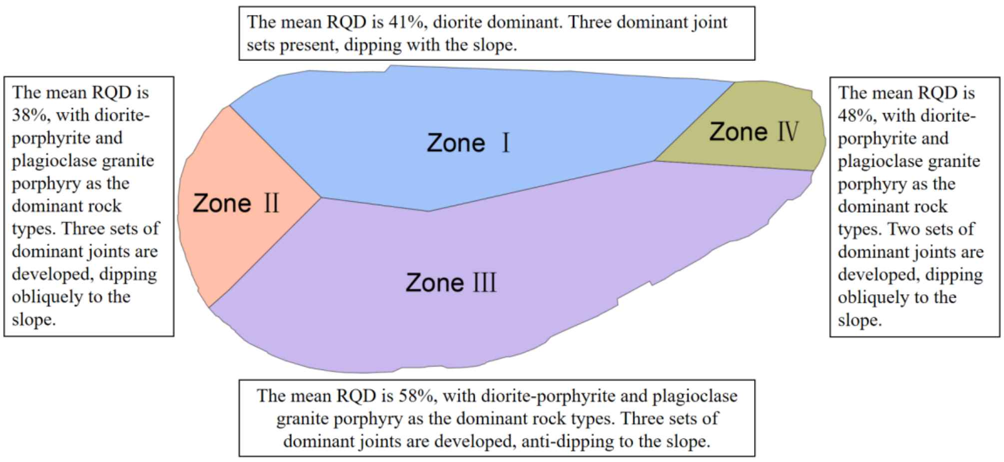

Figure 5 Slope engineering zoning map of Yandong copper mine

According to design, the slope angles for each slope engineering zone are listed in Table 2.

Table 2 Designed pit slope angles

Zone	Designed slope angle (°)	Designed bench slope angle (°)	Remark
I	≤38	≤60	The bench slope angle of the near-surface layer (Quaternary system and weathered layer) shall not exceed 45°
II	≤39	≤60	
III	≤40	≤65	
IV	≤25	≤65	

4.2 Block caving design for underground mining

The mine adopts staged mining. The production scale for Phase I (open pit) and Phase II (underground) is 500× 10^4 t/a. Phase II underground mining commences extraction after the complete completion of Phase I open pit mining. The underground mining design primarily uses the natural caving method, with a development system comprising a belt incline and an auxiliary ramp.

The designed mining scope of Phase II includes remaining orebody resources above the 0 m level and outside the Phase I open pit mining final pit limit; mining below the 0 m level is only planned at this stage. Based on parameters such as the remaining resource quantity outside the open pit and orebody extents, multiple ore drawing schemes were compared using the PCBC software for natural caving method ore drawing. Ultimately, it was determined that the first mining level of underground mining is the +200 m level (with the 0 m level as the subsequent mining level), and the overall mining sequence of the mine is top-down extraction. The vertical projection diagram of the development system is shown in Figure 6.

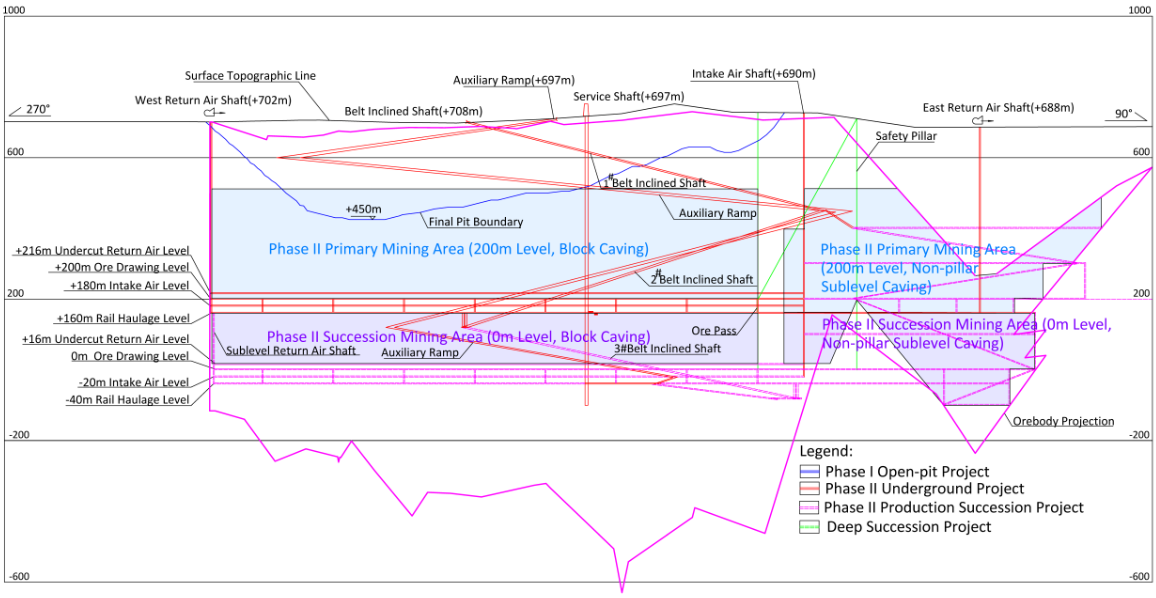

Figure 6 Vertical projection diagram of the development system

When the first mining level of Phase II underground mining is the +200 m level, the following levels are set up: +216 m (undercut and return air level), +200 m (extraction level), +180 m (intake air level), and +160 m (rail haulage level). After extraction of the +200 m level is completed and subsequent mining of the 0 m level commences, the following levels are established: +16 m (undercut and return air level), 0 m (extraction level), −20 m (intake air level), and −40 m (centralised haulage level).

East of Exploration Line 8, the orebody width is relatively narrow and mining in this area is conducted using the pillarless sublevel caving method. The extraction area of the non-pillar sublevel caving method serves as a supplement to the mining output during the reduced production and ramp-up periods resulting from the transition phase of the natural caving method mining area. This is not within the scope of the current study.

5 Simulation of caving process and evolution laws of block caving

5.1 3D mechanical model

After comprehensive consideration, the study determines the numerical simulation domain as follows: east–west length of 5,100 m, north–south width of 4,600 m, bottom elevation of −1,000 m, top elevation bound by the natural ground surface. The main components of the model include the ground surface, orebody, open pit, and hanging wall/footwall surrounding rock. The model is established using a regular hexahedral mesh, with mesh refinement applied in key research areas, resulting in a total of 461,291 nodes and 416,539 elements. The constructed 3D mechanical model is shown in Figure 7.

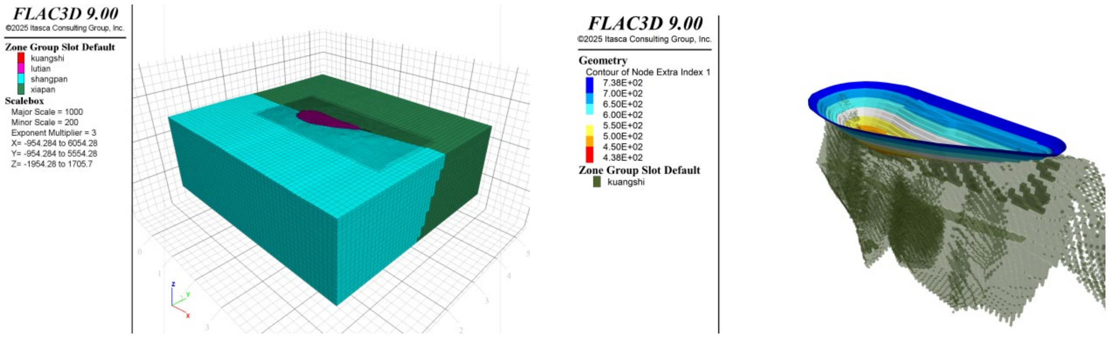

Figure 7 3D model. (a) Axis view; (b) Relationship between open pit and underground ore

5.2 Model construction

5.2.1 Initial in situ stress field and open pit mining simulation

Based on the constructed FLAC3D numerical model, before conducting the simulation calculation of orebody mining, material parameters are assigned according to the corresponding regions in the model, boundary conditions are applied, and the initial in situ stress is calculated. After the calculation reaches equilibrium, the displacement results are cleared and used as the initial in situ stress field for this simulation, which is shown in Figure 8.

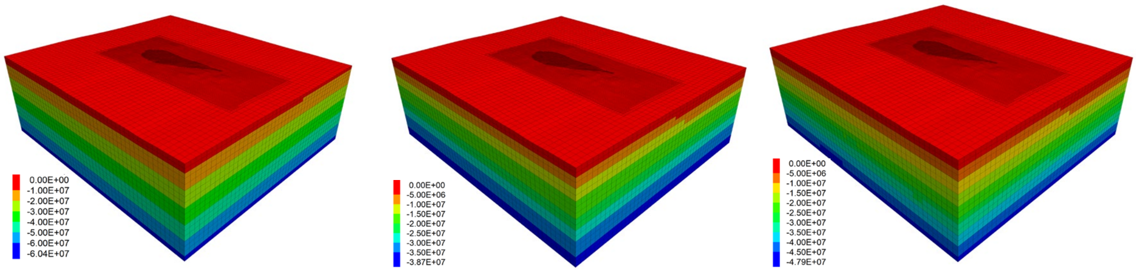

Figure 8 Initial in situ stress. (a) Minimum principal stress; (b) Maximum principal stress; (c) Vertical stress

For the open pit excavation area, the excavation simulation is performed in stages of 50 m each. The simulation employs the Hoek–Brown constitutive model, with the values of elastic parameters and peak strength parameters taken in accordance with the rules of the IMASS constitutive model. After the excavation is completed, the displacement results are cleared and used as the initial state for the cave mining simulation, as shown in Figure 9.

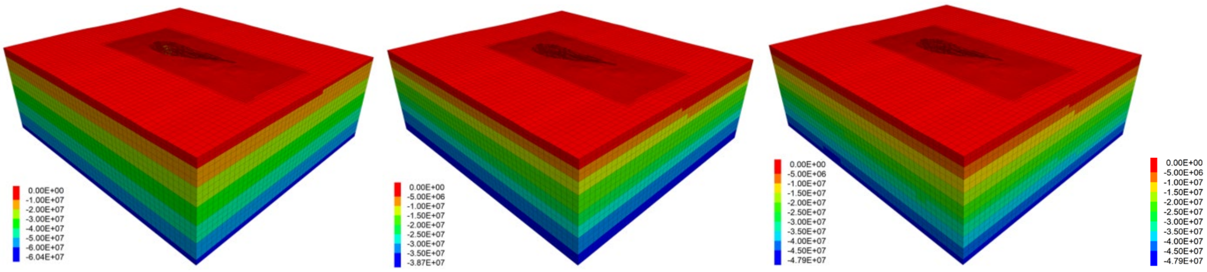

(a) (b) (c)

Figure 9 Post open pit mining stress. (a) Minimum principal stress; (b) Maximum principal stress; (c) Vertical stress

5.2.2 Mechanical parameters of numerical simulation

Based on the research-determined rock mechanics parameters and the assessment results of rock mass quality mechanical parameters, combined with the characteristics of the advanced strain softening constitutive model (IMASS), the finally determined 3D numerical simulation for Yandong copper mine is shown in Table 3.

Table 3 Mechanical parameters for numerical simulation

Engineering rock groups	ρ (g·m^{-3})	E_i (GPa)	GSI	m_i	σ_{ci} (MPa)	M
Diorite porphyrite (hanging wall)	2.82	22.70	59	20	54.02	0.5
Diorite porphyrite (footwall)	2.81	16.74	53	20	44.73	0.5
Plagiogranite porphyry (orebody)	2.71	9.05	51	15	21.34	0.5

5.3 Drawbell process and ore drawing simulation scheme

The drawbell advance rate is 6 m/month, and the ore drawing rate at the ore drawing point is 0.2 m/d. Based on the grid model size of numerical analysis, it is planned that the drawbell front advances 36 m in each calculation stage, equivalent to an actual time of 6 months. A simulation acceleration factor of 10,000 is selected, with the corresponding number of calculation steps per stage being 1,555. The drawpoint extraction rate is 0.023 m/s, the maximum strain rate of the ore drawing unit is 0.18%, and the ore drawing process is a quasi-static process. The drawbell and ore drawing process simulation scheme is shown in Figure 10.

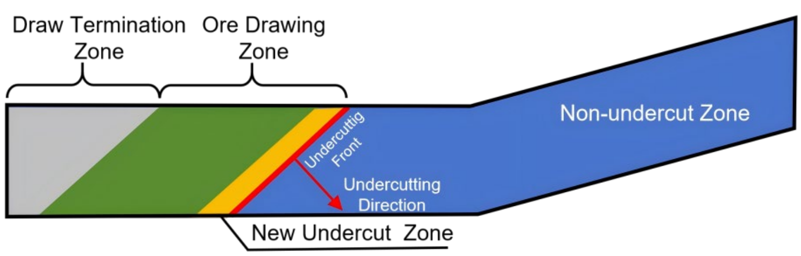

Figure 10 Simulation of drawbell and ore drawing process

Based on the designed drawbell process and empirical ore drawing parameters, the simulation scheme for the drawbell and ore drawing process was determined, and corresponding simulation analyses were conducted, obtaining the development law of rock mass caving, the damage law of rock mass in open pit slopes, and the surface rock movement law.

According to the scope of the drawbell production and ore drawing area in this simulation, the drawbell and ore drawing process simulation scheme set for the 200 m level is divided into 53 calculation stages (Table 4) and the drawbell and ore drawing process simulation scheme set for mining at the 0 m level is divided into 50 calculation stages (Table 5).

Table 4 200 m level drawbell and ore drawing simulation steps

Calculation steps	**1–49**	**50–53**
Drawbell distance (m)	36–1,764	Drawbell ends, continuous ore drawing
Production ore drawing situation	In the layer domain where drawbell has been completed, each ore drawing point continuously conducts ore drawing at a rate of 0.2 m/d.	

Table 5 0 m level drawbell and ore drawing simulation steps

Calculation steps	**54–100**	**101–103**
Drawbell distance (m)	36–1,656	Drawbell ends, continuous ore drawing
Production ore drawing situation	In the layer domain where drawbell has been completed, each ore drawing point continuously conducts ore drawing at a rate of 0.2 m/d.	

The advanced strain softening model (IMASS) was selected for this research. Based on the geomechanical characteristics of the mining scope of the natural block caving method, a three-dimensional engineering geomechanical model of Yandong copper mine was constructed. Functions including bottom ore drawing of the caving method, ore quantity statistics, ore drawing quantity statistics, ore drawing termination, and post-processing analysis methods were established, providing a basis for subsequent simulation studies on the impact of natural block caving at Yandong copper mine on the surface and open pit slopes.

5.3.1 Development law of surface subsidence and caving range

According to simulation calculations, in typical calculation stages where drawbell advance is synchronised with production ore drawing, surface subsidence and the rock mass caving range continuously develop. Among them, red areas represent the rock mass caving range, and white dashed-line areas represent the final boundary of the open pit. The subsidence variation law of rock mass caving during the drawbell process at the 200 m level is shown in Figure 11.

When advanced to 468 m, the slope on the southwest side (hanging wall of the orebody) had completely caved, while the northwest open pit slope (footwall of the orebody) had not yet completely caved, as shown in Figure 11a.

When advanced to 900–1,330 m, the surface caving area spread outward horizontally; the slope near the surface on the northwest side and the northeast slope had not caved, as shown in Figures 11b and 11c.

After the completion of drawbell and ore drawing at the 200 m level, the slope had almost completely caved, with only local remnants left on the northwest side. The main reason is that the final boundary open pit slope of Yandong takes a ‘spoon’ shape, with the bottom of the boundary located on the west side of the mining area. Here, the caving height is relatively low, and the caving contour did not continue to expand outward after developing to the bottom of the boundary, as shown in Figure 11d.

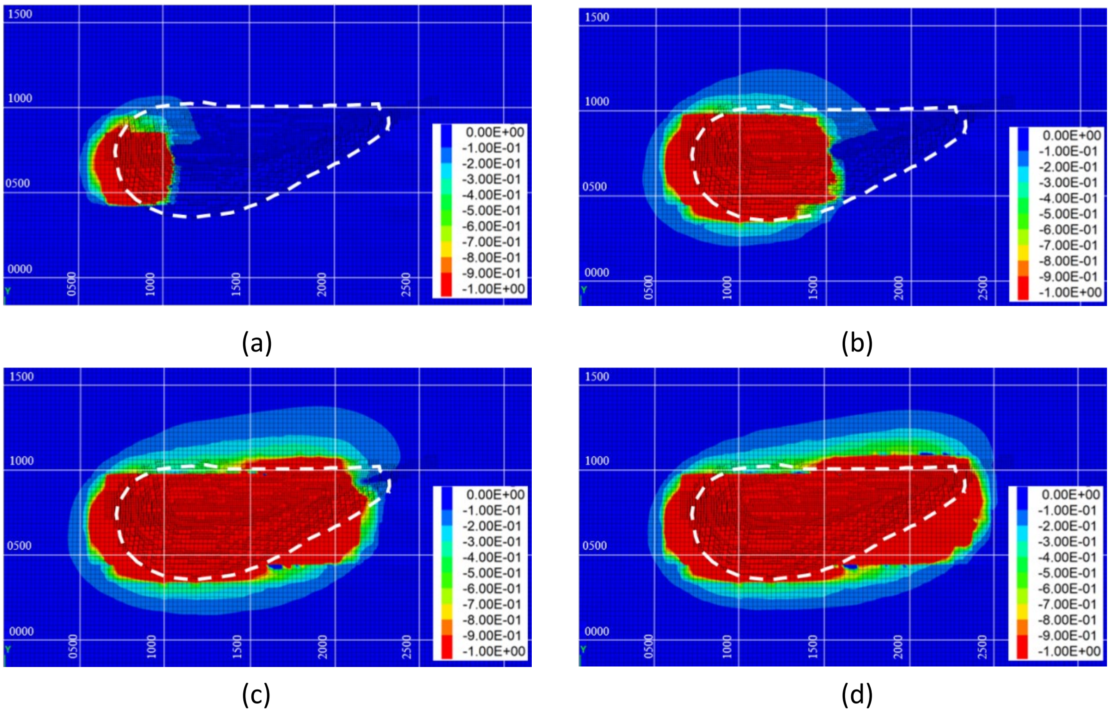

Figure 11 Surface subsidence and slope caving area (red) during the drawbell and ore drawing process at the 200 m level. Drawbell distances (a) 468 m; (b) 900 m; (c) 1,330 m; (d) Post ore drawing

After the completion of drawbell and ore drawing at 0 m level, the surface rock mass caving range further expanded, with both the south and north sides exceeding the southernmost and northernmost ends of the final boundary. Among these, the expansion range of the caving area on the south side was greater than that on the north side, the caving ranges on the east and west sides changed little, and the slope on the northwest side still had not completely caved. The variation law of rock mass caving during the drawbell process at the 0 m level is shown in Figure 12.

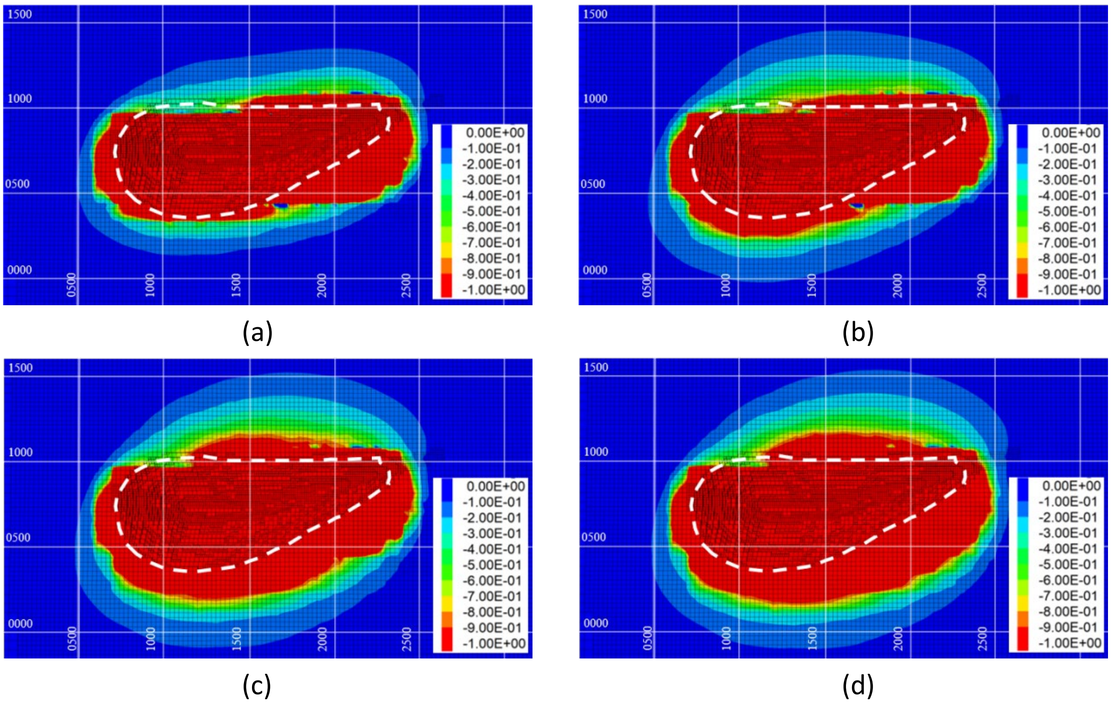

Figure 12 Subsidence and slope caving area (red) during the drawbell and ore drawing process at the 0 m level. Drawbell distances (a) 468 m; (b) 900 m; (c) 1,330 m; (d) Post ore drawing

Following the completion of the drawbell and ore drawing at the 200 m and 0 m levels, the orebody situated above these levels has undergone complete gravitational caving. The spatial relationship between the fully caved material and the open pit is illustrated in Figure 13.

(a) (b)

Figure 13 Spatial relationship between open pit and caved orebody. (a) 200 m level post ore drawing; (b) 0 m level post ore drawing

Figure 13 shows the caved orebody exhibits a distinct inverted funnel geometry, characterised by a bell-shaped profile that propagates continuously and uniformly from the undercut levels upward to the surface. The cave boundary demonstrates remarkable morphological regularity, displaying smooth, consistent contours that gradually expand outward from the extraction points. This uninterrupted funnel configuration indicates favourable capability of the rock mass, thereby facilitating unimpeded flow and full drawdown of the orebody.

5.3.2 Damage evolution of rock mass in open pit slopes

To study the damage law of overlying rock during the mining process, analysis sections were arranged along the strike (Section I-I) and dip direction (Section II-II) of the orebody, as shown in Figure 14a. Figure 14b to Figure 14f show the progression of rock mass damage as the drawbell distance increases. The damage distribution in the figures is interpreted in Table 6.

Table 6 0 m level drawbell and ore drawing simulation steps

Damage value	Physical characteristics
0	The stress in the rock mass of this area has never exceeded its peak strength.
(0, 0.5)	The rock mass in this area has entered the post-peak strain softening stage, but the resulting rock blocks are still fully interlocked with no significant volume expansion.
(0.5, 1)	The rock mass has completely lost its cohesion under unconstrained conditions, rearranges during disturbance and deformation, leading to a rapid increase in voids and permeability.
1	The rock mass in this area is fully broken and expanded during the caving process.

Figure 14b shows that when the drawbell at 200 m level advances to 468 m, the rock mass damage zone in Section I-I expands upward in a step-like manner, and the width of the damage zone gradually expands from the bottom to the top. Significant damage has appeared in the surface rock mass, the damage range on the west side exceeds the final boundary of the open pit slope, and the rock mass at the bottom of the open pit slope begins to experience damage earlier due to stress concentration. Within a certain depth above the drawbell roof, the cohesion of the orebody is effectively reduced to residual strength, and it is essentially in a caved state at this time.

As can be seen from Figures 14c and 14e, during the further advance of the drawbell front line at the 200 m level, rock mass damage and caving above the drawbell roof gradually develop towards the surface and surroundings. At the end of drawbell and ore drawing at the 200 m level, the overall rock mass damage range presents an inverted trapezoidal distribution. The rock mass damage values above the drawbell roof generally reach above 0.9, and the red high-damage zone extends to the bottom of the open pit, forming a continuous caving channel. The surface caving range is basically consistent with the area where rock mass damage exceeds 0.5.

Figures 14d and 14f show that at the end of drawbell and ore drawing at the 0 m level, the shallow damage range is roughly consistent with that at the end of drawbell and ore drawing at the 0 m level. Deep damage only expands above the drawbell roof and near the east and west sides, overall presenting a parabolic shape, indicating that the disturbance of deep rock mass by mining at the 0 m level is spatially constrained in the orebody strike direction.

The rock mass damage range perpendicular to the orebody strike is significantly larger than that along the orebody strike. The main reason is that the Yandong orebody has a tabular shape with steep inclination, and the direction of the maximum principal stress in the mining area intersects the orebody strike at a high angle. This coupling effect between the stress field and the orebody geometry makes the rock mass in the direction perpendicular to the strike more prone to shear slip and tensile fracture. At the end of drawbell and ore drawing at the 200 m level, the overall rock mass damage range presents an inverted trapezoidal distribution, and the damage zone in the orebody dip direction extends farther towards the hanging wall of the open pit slope. At the end of drawbell and ore drawing at the 0 m level, the shallow and deep damage ranges grow synchronously, indicating that the disturbance of deep rock mass by mining at the 0 m level in the direction perpendicular to the orebody strike is not spatially constrained.

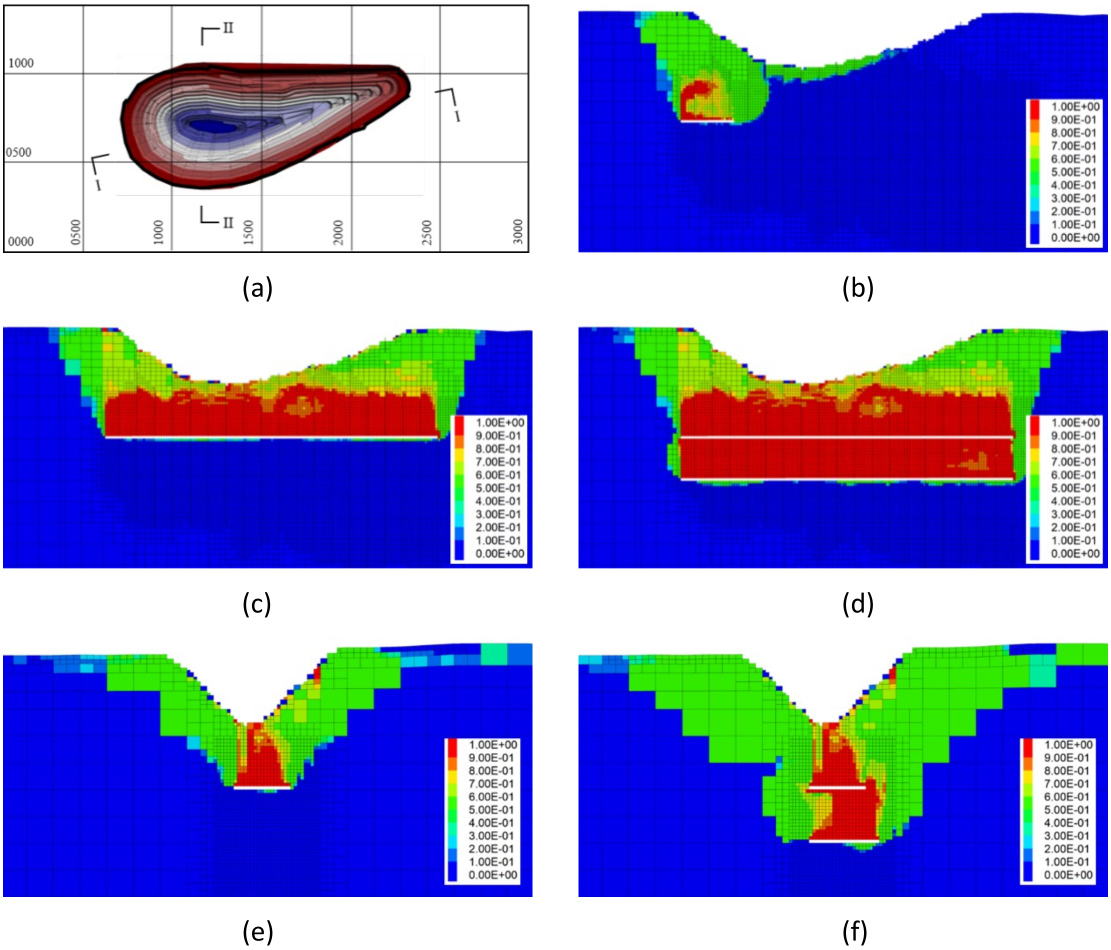

Figure 14 **Damage progression of slope rock mass in typical sections. (a) Section selection; (b) Section I-I 200 m level drawbell distances 468 m; (c) Section I-I: 200 m level, post ore drawing; (d) Section I-I: 0 m level, post ore drawing; (e) Section II-II: 200 m level, post ore drawing; (f) Section II-II: 0 m level, post ore drawing**

6 Conclusion

An engineering geological investigation and caveability evaluation were conducted for the Yandong copper mine area. A statistical analysis of the rock mass quality grades of the orebody and surrounding rock was performed, showing that the rock mass quality of the ore and rock can be divided into three grades: Grade III, Grade IV and Grade V, corresponding to caveability grades of medium, good and very good. According to the evaluation results, the caveability of Yandong copper mine is medium to very good, making it suitable for mining by the natural block caving method. The design adopted a mining method combining open pit mining and natural block caving that aligns with the rock mechanics characteristics.

An engineering geomechanical numerical model of Yandong copper mine was constructed. Using a strain softening constitutive model to simulate the natural block caving mining process, the natural caving evolution laws of ore blocks at the 200 m and 0 m levels during the drawbell and ore drawing processes were revealed, and the following conclusions were drawn:

- After the completion of drawbell and ore drawing at the 200 m level, the slope had almost completely caved, with only the northwest side not yet completely caved. After the completion of drawbell and ore drawing at the 0 m level, the surface rock mass caving range further expanded, with both the south and north sides exceeding the southernmost and northernmost ends of the final boundary. Among these, the expansion of the caving area on the south side was greater than that on the north side, there was minimal change in caving ranges on the east and west sides, and the slope on the northwest side still had not completely caved.
- The disturbance of deep rock mass by mining is spatially constrained in the orebody strike direction. At the end of drawbell and ore drawing at the 0 m level, the shallow damage range along the orebody strike was roughly consistent with that at the end of drawbell and ore drawing at the 0 m level, deep damage only expanded above the drawbell roof and near the east and west sides, overall presenting a parabolic shape. The disturbance in the direction perpendicular to the orebody strike was not spatially constrained. At the end of drawbell and ore drawing at the 0 m level, the shallow and deep damage ranges grew synchronously, and the damage zone in the orebody dip direction extended farther towards the hanging wall of the open pit slope.
- After the completion of mining at the 0 m level of Yandong copper mine, the open pit slope had almost completely caved, with only residual rock mass on the northwest side, and the surface caving range exceeded the final boundary in all directions.

The above caving evolution progression provide a mechanical basis and reference for the mine’s production arrangement and safety control.

Acknowledgement

The authors gratefully acknowledge the National Science and Technology Major Project on Deep Earth (No. 2024ZD1003800), the Science Foundation for Young Scholars of China Minmetals Corporation (No. 2024QNJJA02) and the Science and Technology Special Project of China Minmetals Group (2025ZXA01).

References

Bakhtavar, E, Shahriar, K & Oraee, K 2009, ‘Mining method selection and optimization of transition from open pit to underground in combined mining’, *Archives of Mining Sciences*, vol. 54, no. 3, pp. 481–493.

Brown, ET 2003, *Block Caving Geomechanics*, Julius Kruttschnitt Mineral Research Centre, Indooroopilly.

Brown, ET 2004, ‘Geomechanics: the critical engineering discipline for mass mining’, *MassMin 2004: Proceedings of the 4th International Conference and Exhibition on Mass Mining*, Chilean Engineering Institute, Santiago, pp. 21–36.

Flores, G & Karzulovic, A 2003, *Geotechnical Guideline for a Transition from Open Pit to Underground Mining: Geotechnical Characterization*, report to International Caving Study II, Julius Kruttschnitt Mineral Research Centre, Indooroopilly.

Fu, B, Chu, Y, Zhang, Z, Wei, J & Fu S 2026, ‘Analysis of influence of sublevel caving method from open-pit to underground without pillar on slope stability’, *Journal of Safety Science and Technology*, vol. 22, no. 1, pp. 31–38.

Ghazvinian, E, Garza-Cruz, T, Bouzeran, L, Fuenzalida, M, Cheng, Z, Cancino, C & Pierce, M 2020, 'Theory and implementation of the Itasca constitutive model for advanced strain softening (IMASS)', *Proceedings of the Eighth International Conference and Exhibition on Mass Mining (MassMin 2020)*, University of Chile, Santiago, pp. 451–461.

Laubscher, DH 1994, 'Cave mining - the state of the art', *Journal of the South African Institute of Mining and Metallurgy*, vol. 94, no. 10, pp. 279–293.

Moss, A, Diachenko, S & Townsend, P 2006, 'Interaction between the block cave and the pit slopes at Palabora Mine', *International Symposium on Stability of Rock Slopes in Open Pit Mining and Civil Engineering*, The South African Institute of Mining and Metallurgy, Johannesburg, pp. 399–410.

Pierce, M 2013, 'Numerical modeling of rock mass weakening, bulking and softening associated with cave mining', *47th US Rock Mechanics Geomechanics Symposium*, American Rock Mechanics Association, San Francisco.

Sainsbury, BL 2010, 'Sensitivities in the numerical assessment of cave propagation', in Y Potvin (ed.), *Caving 2010: Proceedings of the Second International Symposium on Block and Sublevel Caving*, Australian Centre for Geomechanics, Perth, pp. 523–535, https://doi.org/10.36487/ACG_rep/1002_36_Bsainsbury

Tegachouang, NC, Bowa, VM, Li, X, Luo, Y & Gong, W 2021, 'Study of the influence of block caving underground mining on the stability of the overlying open pit mine', *Geotechnical and Geological Engineering*, vol. 40, pp. 165–173.

Wang, ML, Li, XS, Wang, YM 2022, 'Stope stability under disturbance in transition of open-pit to underground room and pillar mining', *Mining and Metallurgical Engineering*, vol. 42, no. 2, pp. 32–37.

Wang, Y & Zhong, F 2013, 'Study on slope instability in transition from open-pit to underground mining by similar experiment and numerical simulation', *Journal of China Coal Society*, vol. 38, no. s1, pp. 64–69.

Woo, K, Eberhardt, E & van As, A 2009, 'Characterization and empirical analysis of block caving induced surface subsidence and macro deformations', *3rd Canada-US Rock Mechanics Symposium and 20th Canadian Rock Mechanics Symposium*.

Yuan, K, Ma, C, Guo, G & Wang, P 2024, 'Slope failure of Shilu metal mine transition from open-pit to underground mining Under excavation Disturbance', *Applied Science*, vol. 14, no. 3, 1055.

Zhang, Q, Luo, Y & Ke, Y 2013. 'Security for ground settlement of transition from open pit to underground mining', *Journal of Central South University (Science and Technology)*, vol. 44, no. 8, pp. 3441–3445.